NUMERICAL SIMULATION OF THE EFFECT OF SURFACE CHARGES ON ELECTRON CONFINEMENT IN QUANTUM DOT STRUCTURES *

Minhan Chen and Wolfgang Porod,
Department of Electrical Engineering,
University of Notre Dame,
Notre Dame, IN 46556

Abstract

We present numerical simulations of electron confinement in gated AlGaAs/GaAs quantum dot structures. The confining quantum dot potentials are obtained from solutions of the axisymmetric Poisson equation. Our model takes into account the effect of surface states by viewing the exposed surface as the interface between the semiconductor and the dielectric. We investigate the confining potentials and the dot occupation as a function of different physical models for surface states at the exposed semiconductor surface.

I. INTRODUCTION

In recent years, fabrication techniques have made possible confinement of a two-dimensional electron gas into wires or dots where quantum effects are significant. Typically, such device structures are defined by metallic gates. In order to model electronic confinement in these structures, one has to solve the Poisson and the Schrödinger equations. For solving the Poisson equation, one needs to specify boundary conditions for the potential and/or flux at the exposed semiconductor surface. This is a crucial problem, especially in quantum devices where the confined electrons reside close to the surface. In previous work [1], we have shown that different choices for the boundary conditions at the exposed surface result in noticeable differences for the confining potentials. Highly accurate models of the potential or dielectric flux variation on the exposed semiconductor surface will be needed to realize recently proposed computing architectures for quantum devices, so called Quantum Cellular Automata, which consist of cells of coupled quantum dots in the few electron regime [2].

In our formulation [1], we view as the natural problem domain both the semiconductor and the dielectric, as schematically shown in Fig. 1(a). Thus the usual Dirichlet or Neumann boundary conditions at the exposed semiconductor surface are replaced by more physical matching conditions at the interface between the semiconductor and the dielectric. We assume that the potential is continuous across this interface and that the jump in the normal dielectric flux density is equal to the surface/interface charge density, Q_{int}, which is determined by microscopic models for surface/interface states. We apply our coupled finite-element/boundary-element (FBEM) algorithm to quantum dot structures with axisymmetry. The numerical formulation of the problem is developed in Sec. II and numerical results are presented in Sec. III.

II. PROBLEM FORMULATION

1. Problem Statement

A model quantum dot structure with axisymmetry is shown in Fig. 1. In the semiconductor domain, a quantum dot is realized at the AlGaAs/GaAs heterojunction and is defined by applying a sufficiently nega-

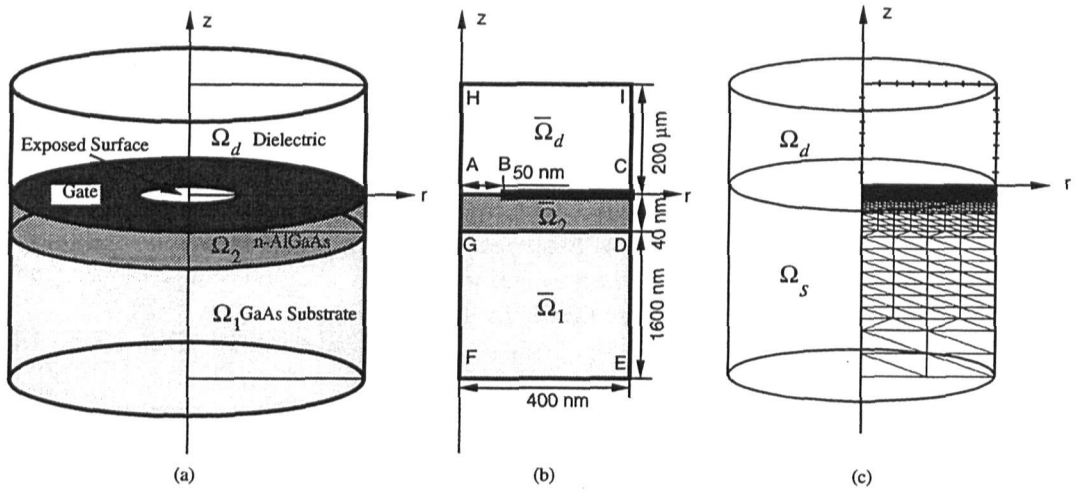

Figure 1: The model quantum dot heterostructure. Fig. 1(a) shows the whole problem domain with axial symmetry which consists of both the semiconductor (Ω_1 and Ω_2) and the dielectric (Ω_d) regions. Fig. 1(b) indicates the two dimensional generating areas and boundaries with typical dimensions. Fig. 1(c) shows the FBEM mesh, which is dense inside the semiconductor region and only consists of the discretized boundary surrounding the dielectric region.

tive gate voltage V_G to the metal gate on the top surface, which contains a circular opening thus exposing the semiconductor surface. For axial symmetry, Poisson's equation can be written in cylindrical coordinates (r,θ,z) as,

$$\frac{1}{r}\frac{\partial}{\partial r}\left(r\varepsilon\frac{\partial u(r,z)}{\partial r}\right)+\frac{\partial}{\partial z}\left(\varepsilon\frac{\partial u(r,z)}{\partial z}\right) = -f[u(r,z)], \tag{1}$$

where $u = (E_C(\phi) - E_F)/kT$ is a reduced variable which measures the separation between the conduction band edge and the Fermi level in units of the thermal energy kT, $f = e\rho/kT$ is the charge density term in the semiconductor, ε is the dielectric constant, and m^* is the effective mass. The generating domains and boundaries are shown in Fig. 1(b).

Equation (1) is a boundary value problem. We solve it by our FBEM algorithm [1], which is a combined finite element method (FEM) for the semiconductor domain and a boundary element method (BEM) for the dielectric region. For the semiconductor domain Ω_s, with $\Omega_s = \Omega_1 \cup \Omega_2$, the standard FEM discretization of equation (1) results in the following non-linear system of equations,

$$\begin{aligned} \boldsymbol{K}_{11}\boldsymbol{u}_o^s + \boldsymbol{K}_{12}\boldsymbol{u}_{BA}^s &= \boldsymbol{P}_f^s, \\ \boldsymbol{K}_{12}^T\boldsymbol{u}_o^s + \boldsymbol{K}_{22}\boldsymbol{u}_{BA}^s &= \boldsymbol{P}_{BA}^s, \end{aligned} \tag{2}$$

where $\boldsymbol{u}_{BA}^s$ and $\boldsymbol{P}_{BA}^s$ contain the potentials and nodal forces at the nodes on the interface $\partial\Omega_{BA}$ between the semiconductor and the dielectric, whereas $\boldsymbol{u}_o^s$ and $\boldsymbol{P}_f^s$ contain the potentials and nodal forces at all other nodes inside the semiconductor domain, and $\boldsymbol{K}$ is the stiffness matrix.

The dielectric domain, Ω_d, is a charge free region. The governing equation is Laplace's equation. Since the fundamental solution of Laplace's equation is known, a boundary integral equation technique can be employed. With the known three dimensional fundamental solution of Laplace's equation in cylindrical coordinates and its associated dielectric flux density [3], the boundary contour $\partial\bar{\Omega}_d$ can be calculated explicitly in terms of complete elliptic integral of the first and second kind, $K(m)$ and $E(m)$, respectively. The resultant system of equations can be expressed as,

$$\begin{aligned} \boldsymbol{S}_{11}\boldsymbol{u}_o^d + \boldsymbol{S}_{12}\boldsymbol{u}_{BA}^d &= \boldsymbol{P}_o^d, \\ \boldsymbol{S}_{21}\boldsymbol{u}_o^d + \boldsymbol{S}_{22}\boldsymbol{u}_{BA}^d &= \boldsymbol{P}_{BA}^d, \end{aligned} \tag{3}$$

where S is the equivalent stiffness matrix, and P^d is the equivalent nodal force vector.

The matching conditions at the exposed surface [1] are given in discretized form by,

$$u^s_{BA} = u^d_{BA} = u_{BA} \quad \text{and} \quad P^s_{BA} + P^d_{BA} = \frac{e}{kT} Q_{int}, \tag{4}$$

where $Q_{int} = Q_{int}(u_{BA})$ is the nodal charge density on the exposed semiconductor surface. A global system of equations is formed by coupling the semiconductor, equation (2), to the dielectric, equation (3), while enforcing the matching conditions (4),

$$\begin{bmatrix} S_{11} & S_{12} & 0 & 0 \\ S_{21} & S_{22} & 0 & I \\ 0 & K_{12} & K_{11} & 0 \\ 0 & K_{22} & K^T_{12} & -I \end{bmatrix} \begin{bmatrix} u^d_o \\ u_{BA} \\ u^s_o \\ P^s_{BA} \end{bmatrix} = \begin{bmatrix} P^d_o \\ Q_{int} \\ P^s_f \\ 0 \end{bmatrix}. \tag{5}$$

Solution of this set yields the potential distribution in the semiconductor and dielectric domains, including the interface $\partial\Omega_{BA}$, and the nodal flux on $\partial\Omega_{BA}$.

2. Interface Charge Density on the Exposed Semiconductor Surface

In order to solve the above problem, the surface charge density, Q_{int}, must be given to specify the matching condition (4). It is known that surface states lying within the energy band gap play a dominant role in the surface charge Q_{int} on exposed semiconductor surfaces [4-6].

In this model, the characters of the surface states are assumed to be acceptor-, D^s_A, and donor-, D^s_D, like. Typical energy distributions of surface states are shown in Fig. 2 [4,5]. The semiconductor surface charge density, as a function of surface potential u_{BA}, is given by Fermi-Dirac statistics with an appropriate quasi-Fermi level for cases of applied bias,

$$Q_{int}(u_{BA}) = -e \int_{E_V}^{E_C} \frac{D^s_A}{1 + exp\,[\,(E - E^s_F)/kT]}\, dE + e \int_{E_V}^{E_C} \frac{D^s_D exp\,[\,(E - E^s_F)/kT]}{1 + exp\,[\,(E - E^s_F)/kT]}\, dE, \tag{6}$$

The strong non-linearity of the surface charge as a function of the potential may cause numerical convergence problems, particularly for low temperatures. We implemented a modified Bank-Rose damping scheme [7] to stabilize the convergence by adaptive underrelaxation and to accelerate the convergence speed of Newton's method. The combination of our coupled finite-element/boundary-element algorithm and the adaptive damping scheme performs quite satisfactorily in our numerical examples.

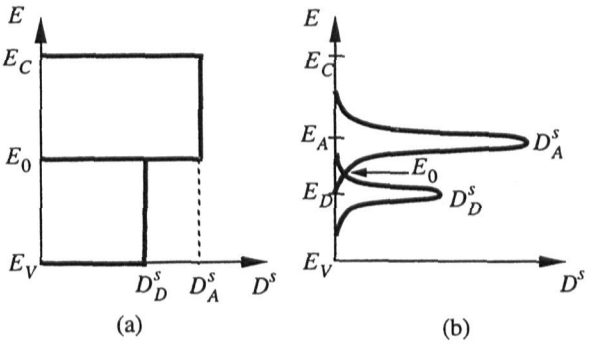

Figure 2: Typical energy distributions of interface states across the semiconductor bandgap; (a) uniform, and (b) localized distributions.

III. NUMERICAL RESULTS

An example heterostructure is shown in Fig. 1 with its relevant physical dimensions indicated. In the

semiconductor domain, a quantum dot is realized at the AlGaAs/GaAs heterointerface by applying a sufficiently negative gate voltage V_G to the patterned metal gate on the top surface. The n-type doping density is assumed to be $10^{18} cm^{-3}$ in the AlGaAs layer and $10^{15} cm^3$ in the GaAs substrate. We assume both uniform and *gaussian* localized energy distributions of surface states across the semiconductor bandgap, as shown in Fig. 2. The characters of the surface states are assumed to be acceptor-, D_A^s, and donor-,D_D^s, like. A semi-classical Thomas-Fermi charge model is assumed in the semiconductor domain.

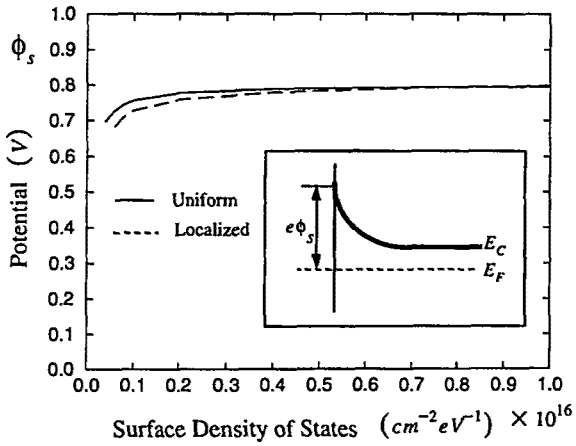

Figure 3: Surface potential ϕ_s on the surface of AlGaAs as a function of the surface density of states for both uniform and gaussian localized energy distributions. Here, $D_A^s = D_D^s$ is assumed.

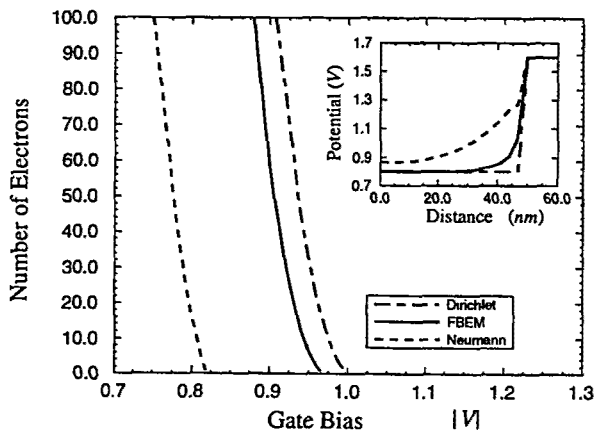

Figure 4: Comparison of the number of confined electrons as a function of gate bias for the three types of boundary conditions on the exposed semiconductor surface. The inset shows surface potential profiles on the semiconductor surface for -0.8 V gate bias.

As shown in Fig. 3, the semiconductor surface potential, ϕ_s, varies with the surface density of states for low defect densities on the surface. For higher surface density of states, however, the surface potential ϕ_s saturates, and the surface Fermi level is then pinned at or near to the energetic position of the neutral level, E_0, shown in Fig. 2. This pinning behavior is observed for both uniform and localized energy distributions of surface states.

Figure 4 presents a comparison of the number of confined electrons as a function of gate bias for different boundary conditions at the exposed semiconductor surface, namely the more conventional Dirichlet and Neumann boundary conditions, and our FBEM matching technique. The parameters and dimensions of the quantum dot structure are the same as those given in Fig. 1. We see that the different formulations produce significantly different results. Specifically, the Dirichlet boundary condition produces a significantly higher number of electrons than the FBEM algorithm, and the Neumann boundary condition produces a much lower quantum dot occupation.

*Supported in part by ARPA/ONR and AFOSR.

[1] M. Chen, W. Porod, and D. J. Kirkner, *J. Appl. Phys.* **75**, 2545 (1994).
[2] C. S. Lent, P. D. Tougaw, W. Porod, and G. H. Bernstein, *Nanotechnology* **4**, 59 (1993).
[3] C. A. Brebbia, J. C. F.Telles, and L. C. Wrobel, *Boundary Element Techniques* (Springer, Berlin, 1984).
[4] A. M. Cowley and S. M. Sze, *J. Appl. Phys.* **36**, 3212 (1965).
[5] W. E. Spicer, I. Lindau, P. Skeath, and Y. Su, *J. Vac. Sci. Technol.* **17**, 1019 (1980).
[6] W. Mönch, Surf. Sci. **132**, 92 (1983).
[7] R. E. Bank and D. J. Rose, *SIAM J. Numer. Anal.* **17**, 806 (1980).